

# Emergent states in dense systems of active rods: from swarming to turbulence

H. H. Wensink<sup>1,2</sup> and H. Löwen<sup>1</sup>

<sup>1</sup> Institut für Theoretische Physik II: Weiche Materie,  
Heinrich-Heine-Universität-Düsseldorf, Universitätsstraße 1, D-40225 Düsseldorf,  
Germany

<sup>2</sup> Laboratoire de Physique des Solides, Université Paris-Sud 11, Bâtiment 510, 91405  
Orsay Cedex, France

E-mail: hlowen@thphy.uni-duesseldorf.de

**Abstract.** Dense suspensions of self-propelled rod-like particles exhibit a fascinating variety of non-equilibrium phenomena. By means of computer simulations of a minimal model for rigid self-propelled colloidal rods with variable shape we explore the generic diagram of emerging states over a large range of rod densities and aspect ratios. The dynamics is studied using a simple numerical scheme for the overdamped noiseless frictional dynamics of a many-body system in which steric forces are dominant over hydrodynamic ones. The different emergent states are identified by various characteristic correlation functions and suitable order parameter fields. At low density and aspect ratio, a disordered phase with no coherent motion precedes a highly-cooperative swarming state at large aspect ratio. Conversely, at high densities weakly anisometric particles show a distinct jamming transition whereas slender particles form dynamic laning patterns. In between there is a large window corresponding to strongly vortical, turbulent flow. The different dynamical states should be verifiable in systems of swimming bacteria and artificial rod-like micro-swimmers.

PACS numbers: 82.70.Dd, 61.30.-v, 61.20.Lc, 87.15.A-

Submitted to: *J. Phys.: Condensed Matter*

## 1. Introduction

Collections of swimming microorganisms and self-propelled particles are able to form remarkable macroscopic patterns [1, 2, 3, 4] including swarms [5, 6] and complex vortices [7, 8, 9, 10, 11]. The tendency for neighbouring particles to align is strongly determined by their mutual interactions which provide the key to understanding the emergent behaviour at high particle density. In this regime, the interplay between microscopic self-motility and anisotropic volume-exclusion interactions leads to complex spatio-temporal behaviour that can be directly visualised in two spatial dimensions, i.e. for particles moving in planar confinement.

Quasi two-dimensional systems of self-propelled particles can be realised in a number of ways. Autonomously navigating bacteria and other microbes can be confined to free-standing thin films [9], between solid surfaces [12] or a liquid-gas interface [8, 13]. On larger length scales, active systems can be realised by polar granular rods on a flat vibrating surface [14, 15] or pedestrians moving in complex environments [16]. Last not least, colloidal dispersions constitute ideal model systems not only for investigating passive matter [17, 18] but also for active matter composed of self-motile colloidal particles. Over the past decade, a number of distinctly different realisations of active colloidal particles have been proposed. These include Janus particles driven by catalytic processes [19, 20] or thermophoretic [21] gradients, particles propelled by artificial flagella [22] and surface waves [23, 24] driven in an external magnetic field. Rather than being spherical most of these particles have an anisotropic rod-like shape which is found to play a crucial role in determining the spatio-temporal behaviour of active particles [25, 26]. Confining systems to quasi-planar geometries allows for a direct visualisation of the particles by means of real-space microscopy and provides fascinating opportunities to study the single-particle and collective behaviour of micro-swimmers.

In this paper we use computer simulation to study a simple model for suspensions of rigid, self-propelled rods (SPR) that interact via a Yukawa-segment potential [27, 28]. The potential allows for a realistic description of the strong mutual short-range repulsion that prevents particles from overlapping. Self-motility is imposed by introducing a constant propulsion force along the main orientation axis of each rod. Consequently, when two neighbouring active rods collide they align and the aligning force plays an essential role in the formation of flocks of coherently moving particles [29]. In our study we focus on the collective behaviour of dense suspensions of strongly interacting particles and characterise the emergent states by analysing different correlation functions as dynamical diagnostics. In order to retain a generic framework we consider the overdamped frictional dynamics of the many-body system where the equations of motion arise from a simple force balance between the Stokesian frictional force, the collision force and the active force on each rod. Likewise, the rod orientations propagate via a torque balance involving the frictional and interaction torque acting on each particle. Other forces due to e.g. many-body hydrodynamic interactions or thermal fluctuations exerted by the embedding solvent are neglected. This allows us to simplify the microscopic

equations of motion in such a way that the rod aspect ratio and density constitute the main variational parameters of the model. The microscopic self-propulsion force can be appropriately scaled out and subsumed into an (effective) Yukawa amplitude which only has a weak impact on the emergent behaviour.

Despite its simplicity the model is capable of predicting a wealth of different steady states that hitherto could not be realised within a single framework. Amongst the various states we identify an incoherent, disordered dynamical phase at small particle aspect ratio and a cooperative swarming state at larger rod anisometry as found in a number of particle-resolved models [29, 25, 28, 30]. At high densities and small aspect ratios, we find a jammed phase with distinct local crystalline order. This state is rather common for passive systems [31] but less obvious for active systems. At large aspect ratio and high density, stratified patterns emerge consisting of lanes driven in opposite directions. These structures are reminiscent of laning patterns observed for mixtures of passive particles (i.e. with no internal driving force) driven in a macroscopic external field [32, 33, 34, 35]. A similar phenomenon was unveiled recently in mixtures of active and passive rod-like particles [36]. For intermediate densities and aspect ratios, we find distinct chaotic states characterised by meso-scale turbulent flow patterns with a significant vorticity in the velocity field [37]. This type of active turbulence has been observed in microbial suspensions [8, 9, 37, 38]. Contrary to traditional turbulent flow observed at high-Reynolds-number passive fluids the vortices that make up the turbulent flow patterns have a uniform mesoscopic size irrespective of the density or particle shape.

In principle, the full variety of different emergent states advanced here should be verifiable for bacterial systems and artificial rod-like colloidal or granular micro-swimmers. In a recent study, the statistical properties of the turbulent states as predicted from the SPR model have been systematically compared with flow-field data of confined bacterial systems [39]. It would be interesting to pursue a more systematic comparison with bacterial systems and assemblies of man-made micro-swimmers in order to verify the full topology of the predicted phase diagram.

The remainder of this paper is organised as follows: in section 2 we specify our model for self-propelled rods, the corresponding equations of motion and the simulation methodology. Numerical results on the non-equilibrium phase diagram are presented and analysed in section 3. We conclude in section 4 with a brief discussion of possible extensions of the model and we highlight opportunities to observe the predicted behaviour in experiment.

## 2. Frictional dynamics of a self-propelled-rod (SPR) model

One of the simplest ways to envisage a suspension of active mesogens is by considering a collection of rigid, self-propelled rods each moving with a constant self-motile force  $F$  directed along the main rod axis (see figure 1). Mutual rod repulsion is implemented by discretising each rod into  $n$  spherical segments and imposing a repulsive Yukawa force with characteristic decay length  $\lambda$  between the segments of any two rods, such that  $\lambda$

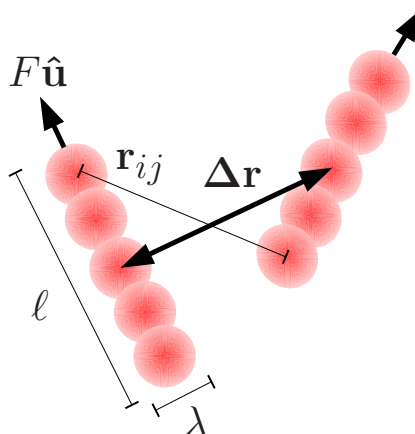


**Figure 1.** Coarse-grained representation of a pair of rod-like micro-swimmers with  $n = 5$  repulsive Yukawa segments and aspect ratio  $a = \ell/\lambda$ . Self-propulsion is provided by a constant force  $F$  acting along the main rod axis indicated by the orientational unit vector  $\hat{\mathbf{u}}$ . The total rod pair potential is obtained by a sum over all Yukawa segment pairs with distance  $\mathbf{r}_{ij}$  and is a function of the centre-of-mass distance vector  $\Delta \mathbf{r}$  and orientations (equation (1)).

defines the effective diameter of the rod of length  $\ell$  [27]. If two sufficiently long rods perform a pair-collision, the interaction results in an effective nematic (apolar) alignment while the centres-of-mass attain a certain minimal distance due to the repulsive Yukawa forces. The potential energy of a rod-pair  $\alpha$  and  $\beta$  with orientation unit vectors  $\{\hat{\mathbf{u}}_\alpha, \hat{\mathbf{u}}_\beta\}$  and center-of-mass distance  $\Delta \mathbf{r}_{\alpha\beta}$ , is given by

$$U_{\alpha\beta} = \frac{U_0}{n^2} \sum_{i=1}^n \sum_{j=1}^n \frac{\exp[-(r_{ij}^{\alpha\beta}/\lambda)]}{r_{ij}^{\alpha\beta}}. \quad (1)$$

where  $U_0$  is the potential amplitude,  $\lambda$  the screening length, and

$$r_{ij}^{\alpha\beta} = |\Delta \mathbf{r}_{\alpha\beta} + (l_i \hat{\mathbf{u}}_\alpha - l_j \hat{\mathbf{u}}_\beta)|, \quad (2)$$

the distance between the  $i$ th segment of rod  $\alpha$  and the  $j$ th segment of rod  $\beta$ , with  $l_i \in [-(\ell - \lambda)/2, (\ell - \lambda)/2]$  denoting the position of segment  $i$  along the symmetry axis of the rod  $\alpha$ . The screening length  $\lambda$  defines the effective diameter of the segments such that we may introduce an aspect ratio  $a = \ell/\lambda$  to quantify the effective anisotropy of the SPR. The case  $a = 1$  corresponds to a single Yukawa point particle ( $n = 1$ ). For  $a > 1$ , the number of segments per rod is fixed as  $n = 3$  for  $1 < a \leq 3$  and  $n = \lfloor 9a/8 \rfloor$  for  $a > 3$  with  $\lfloor \cdot \rfloor$  denoting the nearest integer.

We focus on the dynamical regime relevant to micro-organisms and artificial self-motile colloidal mesogens and we assume the motion of the SPRs to be overdamped due to solvent friction (in the zero Reynolds number limit). Since we are interested in the collision-dominated dynamics in dense suspensions, we disregard thermal and intrinsic fluctuations of e.g. bacterial orientation [4]. Consequently, the equations of motion for the center-of-mass  $\mathbf{r}_\alpha(t)$  and orientation  $\hat{\mathbf{u}}_\alpha(t)$  of each SPR are entirely deterministic

and can be written compactly as

$$\mathbf{f}_T \cdot \partial_t \mathbf{r}_\alpha = -\nabla_{\mathbf{r}_\alpha} U + F \hat{\mathbf{u}}_\alpha, \quad (3)$$

$$\mathbf{f}_R \cdot \partial_t \hat{\mathbf{u}}_\alpha = -\nabla_{\hat{\mathbf{u}}_\alpha} U. \quad (4)$$

Here,  $F$  is a constant self-motility force acting along the longitudinal axis of each rod (figure 1),  $U = (1/2) \sum_{\beta, \alpha: \beta \neq \alpha} U_{\alpha\beta}$  the total potential energy,  $\nabla_{\hat{\mathbf{u}}}$  denotes the gradient on the unit circle, and

$$\mathbf{f}_T = f_0 [f_{\parallel} \hat{\mathbf{u}}_\alpha \hat{\mathbf{u}}_\alpha + f_{\perp} (\mathbf{I} - \hat{\mathbf{u}}_\alpha \hat{\mathbf{u}}_\alpha)], \quad (5)$$

$$\mathbf{f}_R = f_0 f_R \mathbf{I}, \quad (6)$$

are the translational and rotational friction tensors ( $\mathbf{I}$  is the 2D unit tensor) with a Stokesian friction coefficient  $f_0$ . The dimensionless geometric factors  $\{f_{\parallel}, f_{\perp}, f_R\}$  depend solely on the aspect ratio  $a$ , and we adopt the standard expressions for rod-like macromolecules, as given in Ref. [40]

$$\frac{2\pi}{f_{\parallel}} = \ln a - 0.207 + 0.980a^{-1} - 0.133a^{-2}, \quad (7)$$

$$\frac{4\pi}{f_{\perp}} = \ln a + 0.839 + 0.185a^{-1} + 0.233a^{-2}, \quad (8)$$

$$\frac{\pi a^2}{3f_R} = \ln a - 0.662 + 0.917a^{-1} - 0.050a^{-2}. \quad (9)$$

It is expedient to multiply equation (3) with the inverse matrix  $\mathbf{f}_T^{-1}$ :

$$\partial_t \mathbf{r}_\alpha = v_0 \hat{\mathbf{u}}_\alpha - \mathbf{f}_T^{-1} \cdot \nabla_{\mathbf{r}_\alpha} U, \quad (10)$$

where

$$v_0 = \frac{F}{f_0 f_{\parallel}}, \quad (11)$$

defines the self-propulsion velocity of a non-interacting SPR.

In our simulations, we have adopted characteristic units such that  $\lambda = 1$ ,  $F = 1$ , and  $f_0 = 1$ , which means that distance is measured in units of  $\lambda$ , velocity in units of  $F/f_0$ , time in units of  $\tau_0 = \lambda f_0 / F$  and energy in units of  $F\lambda$ . Upon rescaling to dimensionless coordinates, three relevant system parameters remain: The dimensionless Yukawa amplitude  $\tilde{U}_0 = U_0 / (F\lambda)$ , which determines the hardness of the rod interactions relative to their characteristic propulsion energy, the aspect ratio  $a$ , and the effective volume fraction of the system

$$\phi = \frac{N}{A} \left[ \lambda(\ell - \lambda) + \frac{\pi \lambda^2}{4} \right], \quad (12)$$

where the term between brackets denotes the 2D volume  $A_{\text{rod}}$  of a spherocylindrical rod. For steeply repulsive Yukawa interactions, the general dynamical behaviour resembles that of hard rods and does only weakly depend on the Yukawa amplitude, and we fix  $\tilde{U}_0 = 250$ . The remaining quantities, the rod shape  $a$  and volume fraction  $\phi$  constitute the main steering parameters for our investigations. We simulate the evolution of the many-body SPR model as a function of time  $\tau = t/\tau_0$  in a square box of length  $L$

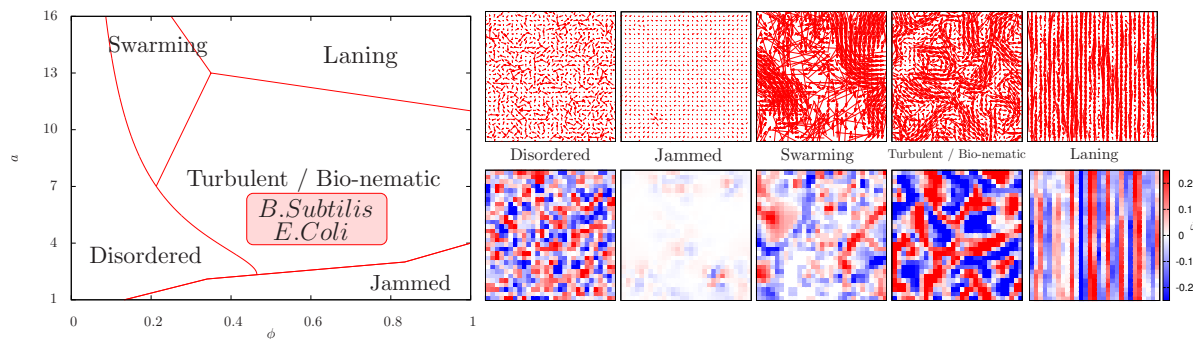


**Figure 2.** Schematic non-equilibrium phase diagram of the 2D SPR model at variable aspect ratio  $a$  and effective filling fraction  $\phi$ . Values exceeding unity are, in principle, possible due to the softness of the Yukawa interactions. The area relevant to self-motile bacteria is highlighted in red. A number of distinctly different dynamical states are discernible as indicated by the coarse-grained maps of the velocity field  $\mathbf{v}(\mathbf{r}, t)$  (upper panels) at time  $t$  and the corresponding scalar vorticity field  $\tilde{\omega}(\mathbf{r}, t) = [\nabla \times \mathbf{v}(\mathbf{r}, t)] \cdot \hat{\mathbf{e}}_z$  (lower panels) expressed in units of  $\tau_0^{-1}$ .

with periodic boundary conditions at volume fractions in the range  $0.05 < \phi < 0.9$ . The simulations are carried out using a time discretisation  $\Delta\tau = 0.002\rho^{-1/2}$ , where  $\rho = N\lambda^2/A$  with typically  $N = 10^4$  and rods per simulation. Initial configurations, generated from a rectangular lattice of aligned rods with  $\hat{\mathbf{u}}$  pointing randomly up or down are allowed to relax during an interval  $\tau = 1000$  before statistics is being gathered over an interval  $\tau = 20L$  with  $L = (N/\rho)^{1/2}$  the dimension of the simulation box (in units of  $\lambda$ ). Velocity vector fields  $\mathbf{v}(\mathbf{r}, t)$  are constructed by measuring the average centre-of-mass velocity within small sub-cells centered around the position  $\mathbf{r}$ . To this end we project the particle positions onto a 2D cubic grid  $\{(i, j) \mid 1 \leq i, j \leq G\}$  and measure the average velocity  $\mathbf{v}(t; i, j)$  in each bin  $(i, j)$  at a given time  $t$ . In order to test for finite size effects, we consider two different system sizes: ‘small’ systems with  $N = 1 \cdot 10^4$  particles and ‘large’ systems with  $N = 4 \cdot 10^4$  particles at the same filling fraction  $\phi$ . The coarse-graining parameter  $G$  is chosen adaptively such as to ensure each bin to represent the average velocity of about 10 SPRs. Generally, we observe that the dynamical structure and order parameters of the emergent states are robust with respect to changes in the particle number  $N$ , provided  $N$  is at least of  $\mathcal{O}(10^4)$ .

### 3. Results

#### 3.1. Non-equilibrium phase diagram for the SPR model

Upon varying the effective volume filling fraction  $\phi$  and the rod aspect ratio  $a$  a number of qualitatively different dynamical phases emerge. A schematic non-equilibrium phase diagram, shown in figure 2, illustrates the importance of the SPR anisometry in determining the stationary dynamical state of the system. The low density regime is generally characterised by disordered dynamics with little or no cooperative motion. Beyond a certain threshold density cooperative motion becomes manifest and translates

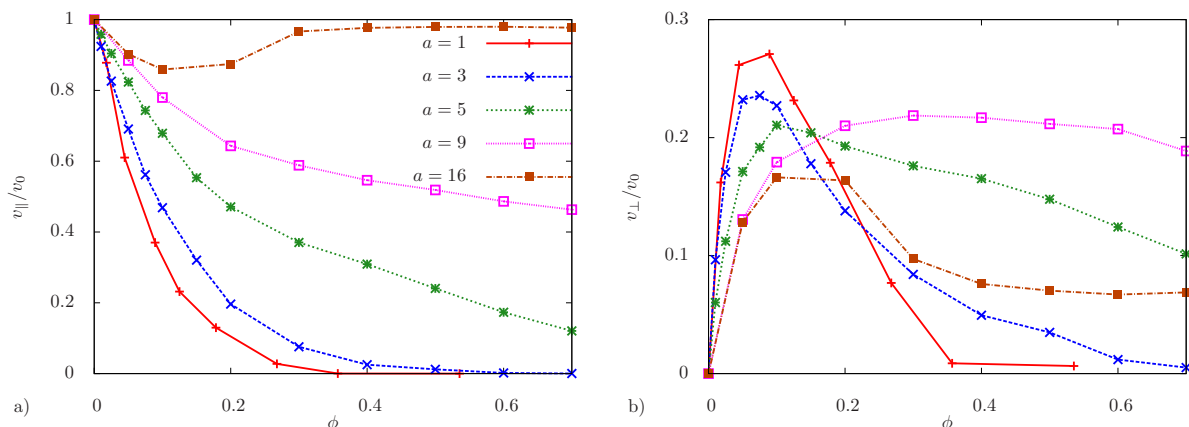


**Figure 3.** Evolution of the average SPR velocity as a function of filling fraction  $\phi$  for a number of particle aspect ratios. Shown is the average velocity component  $v_{\parallel}$  along the main rod orientation (a) and the average perpendicular component  $v_{\perp}$  (b), both expressed in units of the velocity  $v_0$  of a free SPR.

into dynamical states whose structure depends on the intrinsic ‘aligning force’ of the SPRs. Short rods generally jam at high packing fractions whilst very long rods ( $a > 13$ ) exhibit swarming behaviour with large spatio-temporal density fluctuations. The swarming and laning phases adjoin a large region of bio-nematic and turbulent flow characterised by vortices and extended nematic jet-like structures [37, 41].

Generally, the transitions from the dilute phase to regimes with strong cooperative motion can be localised by the 2D Onsager overlap density [42], defined as the density corresponding to a single rod occupying an average area equal to its excluded area  $A_{\text{ex}} = (2/\pi)(\ell - \lambda)^2 + (\pi/4)\lambda^2$ . The latter expression can be derived from the rod dimensions in figure 1 by assuming a pair of spherocylindrical rods with isotropic orientations. By combining terms one arrives at the following expression for the overlap density:

$$\phi^* = \frac{A_{\text{rod}}}{A_{\text{ex}}} = \frac{1 + 4(a - 1)/\pi}{1 + 8(a - 1)^2/\pi^2}. \quad (13)$$

This quantity delimits the density regime beyond which many-body rod collisions (exceeding the pair level) are starting to become important and various non-trivial emergent states arise. In the sections below we shall discuss these in more detail.

### 3.2. Short rods: active jamming

For small aspect ratios  $a > 3$  a distinct transition towards a jammed state is observed upon increasing density. This behaviour is hinted at by the average SPR velocity for which we may probe both parallel and transverse contributions via

$$v_{\parallel} = \frac{1}{N} \left\langle \sum_{\alpha=1}^N \hat{\mathbf{u}}_{\alpha} \hat{\mathbf{u}}_{\alpha}(t) \cdot \mathbf{v}_{\alpha}(t) \right\rangle,$$

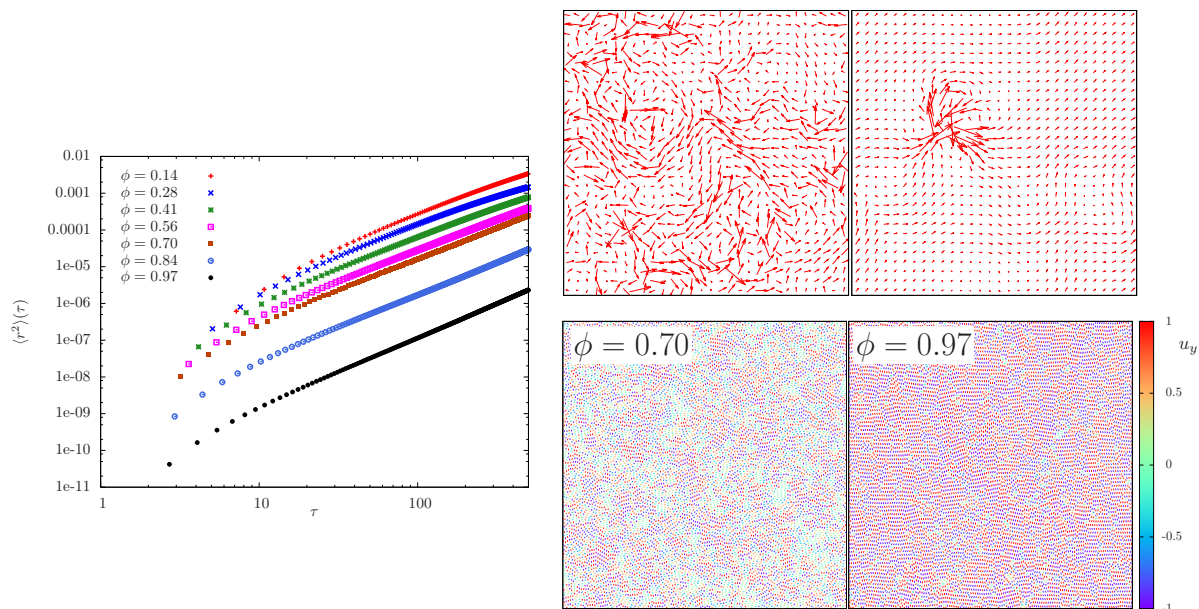


**Figure 4.** Mean-square displacement of the centre-of-mass for SPRs with aspect ratio  $a = 3$ . The snapshots depict velocity fields (upper panels) and the SPR coordinates (lower panels) for two different bulk filling fractions corresponding to a dynamically disordered fluid at  $\phi = 0.70$  and a jammed state at  $\phi = 0.97$ . Colour coding is used to indicate the orientation  $u_y = \hat{\mathbf{u}} \cdot \hat{\mathbf{e}}_y$  of each rod.

$$v_{\perp} = \frac{1}{N} \left\langle \sum_{\alpha=1}^N (\mathbf{I} - \hat{\mathbf{u}}_{\alpha} \hat{\mathbf{u}}_{\alpha}(t)) \cdot \mathbf{v}_{\alpha}(t) \right\rangle, \quad (14)$$

where the brackets  $\langle \dots \rangle$  denote a time average. The results are depicted in figure 3. In general, the average parallel velocity decreases monotonically with density as the particles get progressively hindered in their motion due to mutual rod collisions. For small  $a$  the mobility drops rapidly for larger  $\phi$  until reaching a threshold level at virtually  $v_{\parallel} \sim 0$  indicating dynamical arrest. This behaviour is more clearly reflected in the mean-square displacement (figure 4) where a sharp drop in the mobility (over nearly 2 orders of magnitude) at  $\phi = 0.84$  marks the onset of jamming. Throughout the density range the motion is observed to be sub-ballistic at long times with  $\langle r^2 \rangle \sim \tau^{1.75 \pm 0.1}$ . The jamming point depends strongly on particle anisometry as indicated in figure 2 with a marked shift towards higher volume fractions upon increasing  $a$ . From a structural point of view the jamming transition is accompanied by a crossover towards orientationally and positionally ordered structures as evident from the marked degree of local crystalline order at large filling fractions. The velocity maps reveal small pockets of locally enhanced particle mobility that point to the presence of dynamical heterogeneities as commonly found in glassy systems at finite temperature. A detailed account of freezing and glassy behaviour of self-motile spherical Yukawa particles has been reported in Ref. [43].



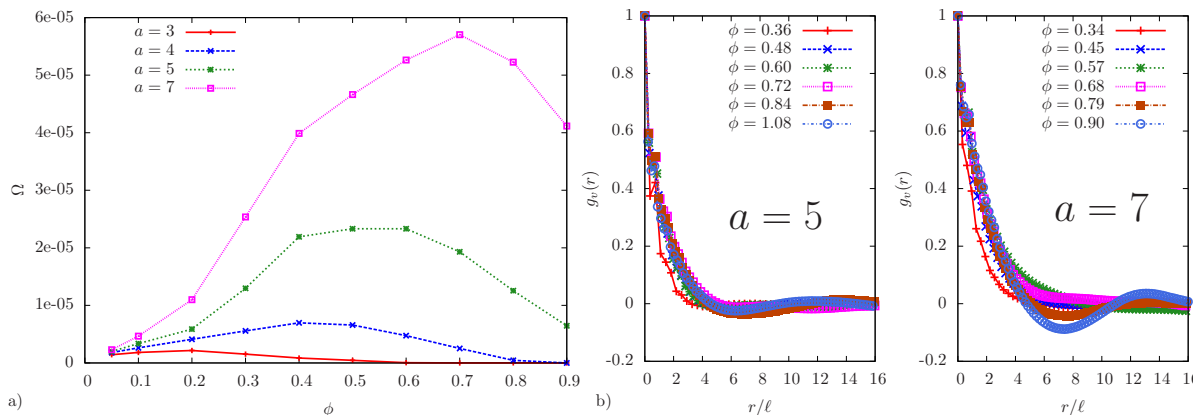


**Figure 5.** (a) Enstrophy  $\Omega$  (in units  $\tau_0^{-2}$ ) versus filling fraction for a number of aspect ratios  $a$  in the turbulent regime. The maxima correspond to the densities where mixing due to vortical motion is the most efficient. (b) Spatial velocity autocorrelation function for a number of bulk volume fractions in the turbulent flow regime for two different aspect ratios  $a$ .

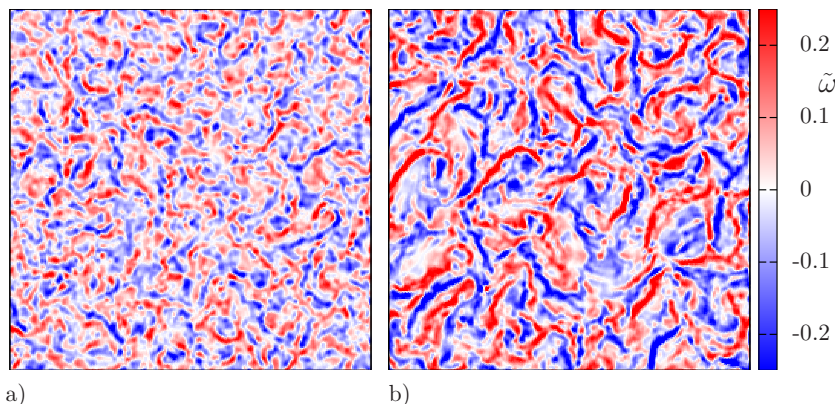


**Figure 6.** Maps of the vorticity field  $\tilde{\omega}(\mathbf{r}, t) = [\nabla \times \mathbf{v}(\mathbf{r}, t)] \cdot \hat{\mathbf{e}}_z$  expressed in units of  $\tau_0^{-1}$  showing large-scale turbulent flow for SPRs at intermediate aspect ratios: (a)  $\phi = 0.72$ ,  $a = 5$  and (b)  $\phi = 0.90$ ,  $a = 7$ . The snapshots are based on  $N = 4.10^4$  SPRs. The lateral box dimensions are  $103\ell$  (a) and  $78\ell$  (b).

### 3.3. Intermediate aspect ratio: vortical states and turbulence

The maximum in the transverse SPR velocities depicted in figure 3b suggest that the SPRs exhibit some degree of collective swirling motion at moderate densities even at small aspect ratios. This type of motion becomes much more manifest at larger  $a$  where distinct vortical patterns arise akin to turbulent flow. The kinetic energy associated with local vortical motion can be measured from the *enstrophy* per unit area [44, 45, 46] which is defined as:

$$\Omega = \frac{1}{2} \left\langle \overline{|\tilde{\omega}(\mathbf{r}, t)|^2} \right\rangle, \quad (15)$$

where the overbar denotes a spatial average. For slender rods ( $a \geq 3$ ) the mean enstrophy exhibits a pronounced maximum as a function of the volume fraction  $\phi$  (figure

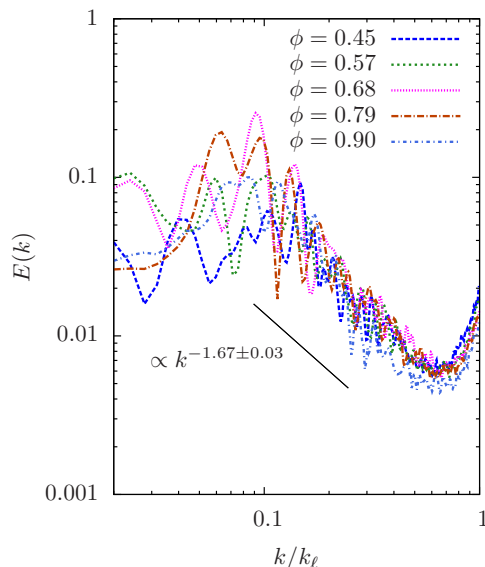


**Figure 7.** Power spectra of the kinetic energy for turbulent flow of SPRs with  $a = 7$  ( $k_\ell = 2\pi/\ell$ ). Universal scaling behaviour (with scaling exponent  $-5/3$ ) is observed in the intermediate range of wavenumbers  $k$ .

5b). This maximum signals the density at which vortical motion is maximal. In a bacterial suspension this extremum would correspond to the optimal concentration for fluid mixing. The range of aspect ratios over which turbulence flow is stable corresponds well with the typical aspect ratios of bacterial cell bodies, e.g.  $a \sim 3$  for *E. Coli* and  $a \sim 6$  for *B. subtilis* (cf. figure 2).

The typical size of the vortices that make up the turbulent flow patterns can be extracted from the equal-time velocity autocorrelation function (VACF)  $g_v(r) = \langle \mathbf{v}(0, t) \cdot \mathbf{v}(\mathbf{r}, t) \rangle$ . This quantity can be obtained from the microscopic SPR coordinates  $\{\mathbf{r}_\alpha, \mathbf{v}_\alpha\}$  via:

$$g_v(r) = \frac{\left\langle \sum_\alpha \sum_{\beta \neq \alpha} \delta(r - |\mathbf{r}_\alpha - \mathbf{r}_\beta|) (\mathbf{v}_\alpha \cdot \mathbf{v}_\beta - \langle v \rangle^2) \right\rangle}{\left\langle \sum_\alpha \sum_{\beta \neq \alpha} \delta(r - |\mathbf{r}_\alpha - \mathbf{r}_\beta|) (\langle v^2 \rangle - \langle v \rangle^2) \right\rangle}. \quad (16)$$

The decay of the VACFs in figure 5b reveals a typical vortex size of about  $\sim 5\ell$ , an estimate that seems rather insensitive to the bulk density and aspect ratio. Monotonically decreasing velocity correlations correspond to bio-nematic-type states where large-scale nematic jets and vortices coexist [37] whereas negative correlations (cf. the curves for  $a = 7$  and  $\phi > 0.8$ ) represent more pronounced vortical collective motion reminiscent of fully developed meso-scale turbulent flow [39]. Typical vorticity snapshots are shown in figure 6.

In order to make a connection with classical 2D turbulence in high-Reynolds number fluids we have calculated the energy spectrum which can be obtained as a Fourier transform of the VACF:

$$E(k) = \frac{k}{2\pi} \int d\mathbf{r} \exp[-i\mathbf{k} \cdot \mathbf{r}] \langle \mathbf{v}(0, t) \cdot \mathbf{v}(\mathbf{r}, t) \rangle. \quad (17)$$

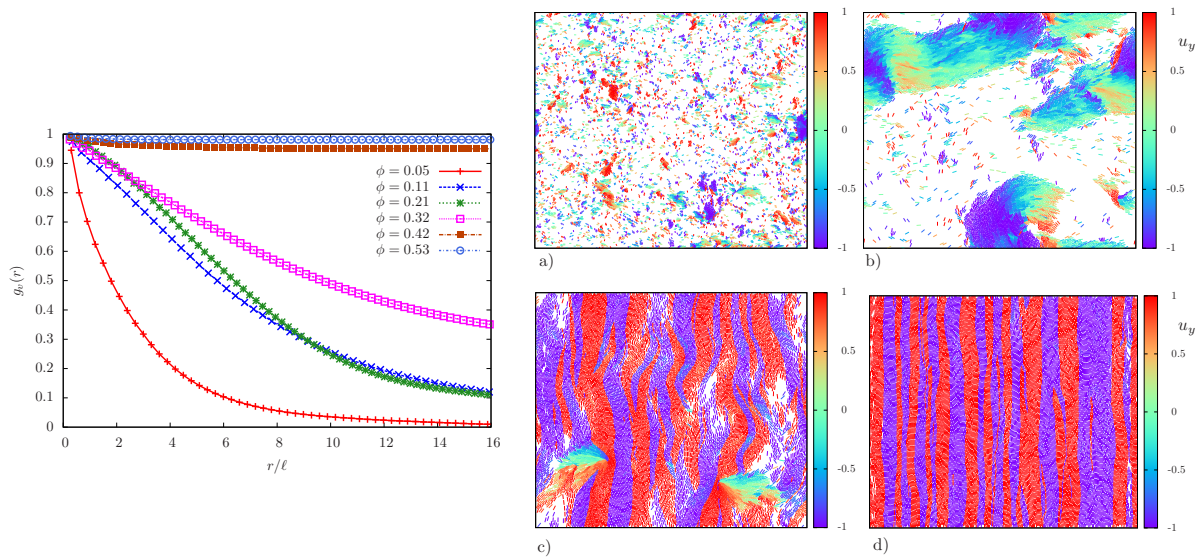


**Figure 8.** Spatial auto-correlation functions of the vertical velocity component  $g_{v_y}(r)$  (equation (16)) at various filling fractions  $\phi$  for SPRs with  $a = 16$ . Particle snapshots of the stationary states at (a)  $\phi = 0.05$  - disordered, incoherent motion (b)  $\phi = 0.21$  - swarming, (c)  $\phi = 0.32$  - initial stage of laning formation, and (d)  $\phi = 0.42$  - fully developed laning state. The lateral box dimension corresponds to  $38\ell$ . Colour coding is used to indicate the orientation  $u_y = \hat{\mathbf{u}} \cdot \hat{\mathbf{e}}_y$  of each rod.

An alternative and more formal definition reads  $\langle v^2 \rangle = 2 \int_0^\infty dk E(k)$  where  $E(k)$  reflects the accumulation of kinetic energy over different length scales. The results in figure 7 suggest asymptotic power law scaling regimes for intermediate  $k$ -values with a power-law exponent close to the characteristic  $k^{-5/3}$ -decay predicted by the Kolmogorov-Kraichnan scaling theory [47, 48] for (passive) 2D turbulence in the inertial regime. In the present case, however, inertia is absent on the particle scale because the SPR motion is completely overdamped but it is possible that the self-propulsion establishes ‘effective’ collective inertial effects on larger scales which could explain the observed  $k^{-5/3}$  decay. Contrary to regular turbulent flow where energy is injected on the macroscopic scale, active turbulence is characterised by forcing on the microscopic scale. In general, the transport of kinetic energy towards smaller  $k$  becomes significantly damped on larger length scales [13] as highlighted by the low- $k$  plateau in the power spectra in figure 7. We refer the reader to Ref. [39] for a more detailed discussion comparing meso-scale turbulence in active suspensions and regular high-Reynolds-number turbulent flow.

### 3.4. Long rods: swarming and lane formation

At low to moderate density slender rods with  $a > 10$  tend to form large compact flocks reminiscent of the cooperative motion observed in large groups of organisms, e.g. fish schools, bird flocks (see figure 8a-b) [49, 50]. At larger volume fractions distinct laning patterns emerge that consist of cooperative stratified motion (figure 8c-d). The transition from flocking to laning as a function of the volume fraction can be localised

from the equal-time VACF for the velocity components along the lane directions (in this case the vertical  $y$ -component). The characteristic decay of the VACF  $g_{v_y}(r)$ , shown in figure 8, allows a distinction between the disordered state at low densities where rod clusters are small and velocity correlations decay rapidly and the emergence of large cooperative flocks with velocity correlations spanning several dozens of rod lengths. A marked divergence of the correlation length occurs around  $\phi \approx 0.4$  where the flocks start to span the entire system and self-organise into lanes moving in opposite directions. The laned patterns remain stable throughout the sampled time interval and no sign of break-up is observed over time even for large systems. We have verified the stability of the lanes against small thermal fluctuations of the rod orientations that could be induced by the embedding medium or by some internal source, e.g., bacterial flagella. The rotational fluctuations are represented by a Gaussian white noise contribution  $\Delta\hat{\mathbf{u}}$  to the equation of rotational motion of each rod  $\alpha$  (cf. equation (4)):

$$\partial_t \hat{\mathbf{u}}_\alpha = -\mathbf{f}_R^{-1} \cdot \nabla_{\hat{\mathbf{u}}_\alpha} U + \Delta\hat{\mathbf{u}}_\alpha. \quad (18)$$

The stochastic term has zero mean  $\langle \Delta\hat{u}_{i\alpha} \rangle = 0$  and correlations  $\langle \Delta\hat{u}_{i\alpha}(t) \Delta\hat{u}_{j\beta}(t') \rangle = 2D_R^* \delta_{ij} \delta_{\alpha\beta} \delta(t - t')$  (with  $i = x, y$ ) in terms of some effective rotational diffusion rate  $D_R^*$ . Although ‘run-and-tumble’ motion as commonly observed in bacterial systems (notably *E. Coli* [4, 51]) is strictly non-Brownian at short times, its long-time behaviour is well-captured by a rotational diffusion process with a diffusion constant much larger than the Stokes-Einstein value  $D_R = k_B T / f_0 f_R$  (where  $k_B T$  is the thermal energy) for passive Brownian rods [51]. The strength of the tumbling motion is conveniently expressed in terms of the dimensionless tumbling parameter  $\ell D_R^* / v_0$  which is the ratio of the translation time a free SPR needs to swim over a distance  $\ell$  and the typical tumbling time  $1/D_R^*$ . Typical values for *E. Coli* and other swimming bacteria are  $\ell D_R^* / v_0 \sim 0.01$  [4]. In the dense regime, the particle velocities are dominated by rod-rod collisions rather than thermal fluctuations and the intrinsic rotational diffusivity of the SPRs does not incur any qualitative change to the laning structures. In general, we assume that the spatio-temporal states and the topology of the phase diagram is robust against weak fluctuations in the swimming direction of the SPRs. We remark that similar laning states were encountered at finite temperature in binary mixtures of SPRs with different self-motility [36]. In both classes of driven systems laning instabilities occur if the disparity between the species mobility exceeds a certain threshold. In our case, however, such an intrinsic driving force is absent since all particles have equal mobility.

#### 4. Conclusions

We have studied the collective dynamical behaviour of a simple two-dimensional model of self-propelled rigid rods (SPR) by means of numerical simulation. Depending on the rod shape and density, the SPR model exhibits a wealth of different emergent dynamical states including swarming, turbulence, laning and jamming. Although many of these states have been encountered in various set-ups, most notably (mixtures of)

spherical particles in different external fields, the SPR model is able to generate these dynamical states upon variation of only two basic system parameters; the particle shape and density. The present approach may therefore serve as a benchmark to characterise the collective properties of different classes of self-motile organisms and artificial microswimmers of various shapes. As for the turbulent state, it was recently shown that the SPR model is capable of reproducing the velocity statistics obtained from experiments on strongly confined *Bacillus subtilis* suspensions [39]. Future experiments on dense systems of self-propelled particles with low and high particle anisometry will hopefully allow for similar comparisons for the jammed and laned state, respectively.

Future efforts could be aimed at extending the SPR model and the associated equations of motion by accounting for e.g. multi-body hydrodynamic interactions mediated by the solvent, particle flexibility and body forces transmitted by chemical gradients (chemotaxis) that could be relevant in concentrated bacterial systems. The influence of thermal fluctuations could be incorporated if one wishes to assess the effect of translation and rotational noise (bacterial tumbling) in more detail. It is also desirable to explore the SPR model in three spatial dimensions, for instance, to study the phenomenology of fully developed 3D meso-scale active turbulent flow which has been unexplored so far. Finally, it would be challenging to construct microscopic theories that are capable of predicting the observed emergent states advanced in this study. Dynamical density functional theory for anisotropic particles [28, 52, 53] could provide a promising avenue for this.

## Acknowledgments

We are grateful to Jörn Dunkel and Lyderic Bocquet for helpful discussions. Financial support from the DFG within SFB TR6 (project D3) is gratefully acknowledged.

## References

- [1] Copeland M F and Weibel D B 2009 *Soft Matter* **5** 1174–1187
- [2] Koch D L and Subramanian G 2011 *Annual Review of Fluid Mechanics* **43** 637–659
- [3] Sokolov A and Aranson I S 2009 *Phys. Rev. Lett.* **103** 148101
- [4] Drescher K, Dunkel J, Cisneros L H, Ganguly S and Goldstein R E 2011 *Proc. Natl. Acad. Sci. USA* **108** 10940–10945
- [5] Kearns D B 2010 *Nature Rev. Microbiol.* **8** 634–644
- [6] Ramaswamy S 2010 *Annual Rev. Cond. Mat. Phys.* **1** 323–345
- [7] Berg H C 2000 *Physics Today* **53** 24–29
- [8] Dombrowski C, Cisneros L, Chatkaew S, Goldstein R E and Kessler J O 2004 *Phys. Rev. Lett.* **93** 098103
- [9] Sokolov A, Aranson I S, Kessler J O and Goldstein R E 2007 *Phys. Rev. Lett.* **98** 158102
- [10] Riedel I H, Kruse K and Howard J 2005 *Science* **309** 300–303
- [11] Saintillan D and Shelley M 2008 *Phys. Fluids* **20** 123304
- [12] Miño G, Mallouk T E, Darnige T, Hoyos M, Dauchet J, Dunstan J, Soto R, Wang Y, Rousselet A and Clement E 2011 *Phys. Rev. Lett.* **106** 048102

- [13] Ishikawa T, Yoshida N, Ueno H, Wiedeman M, Imai Y and Yamaguchi T 2011 *Phys. Rev. Lett.* **107** 028102
- [14] Volfson D, Kudrolli A and Tsimring L S 2004 *Phys. Rev. E* **70** 051312
- [15] Narayan V, Ramaswamy S and Menon N 2007 *Science* **317** 105–108
- [16] Helbing D, Farkas I and Vicsek T 2000 *Nature* **407** 487–490
- [17] Löwen H 2001 *J. Phys.: Condensed Matter* **13** R415–R432
- [18] Löwen H 2008 *J. Phys.: Condensed Matter* **20**
- [19] Erbe A, Zientara M, Baraban L, Kreidler C and Leiderer P 2008 *J. Phys.: Condens. Matter* **20** 404215
- [20] Palacci J, Cottin-Bizonne C, Ybert C and Bocquet L 2010 *Phys. Rev. Lett.* **105** 088304
- [21] Volpe G, Buttinoni I, Vogt D, Kummerer H J and Bechinger C 2011 *Soft Matter* **7** 8810
- [22] Dreyfus R, Baudry J, Roper M L, Fermigier M, Stone H A and Bibette J 2005 *Nature* **437** 862
- [23] Snezhko A, Belkin M, Aranson I S and Kwok W K 2009 *Phys. Rev. Lett.* **102** 118103
- [24] Snezhko A and Aranson I S 2011 *Nature Materials* **10** 698–703
- [25] Peruani F, Deutsch A and Bär M 2006 *Phys. Rev. E* **74** 030904
- [26] Peruani F, Starruß J, Jakovljevic V, Søgaard-Andersen L, Deutsch A and Bär M 2012 *Phys. Rev. Lett.* **108** 098102
- [27] Kirchhoff T, Löwen H and Klein R 1996 *Phys. Rev. E* **53** 5011–5022
- [28] Wensink H H and Löwen H 2008 *Phys. Rev. E* **78** 031409
- [29] Vicsek T, Czirók A, Ben-Jacob E, Cohen I and Shochet O 1995 *Phys. Rev. Lett.* **75** 1226–1229
- [30] Yang Y, Marceau V and Gompper G 2010 *Phys. Rev. E* **82** 031904
- [31] Liu A J and Nagel S R 1998 *Nature* **396** 21–22
- [32] Dzubiella J, Hoffmann G P and Löwen H 2002 *Phys. Rev. E* **65** 021402
- [33] Rex M and Löwen H 2008 *Eur. Phys. J. E* **26** 143–150
- [34] Wysocki A, R ath C, Ivlev A V, S utterlin K R, Thomas H M, Khrapak S, Zhdanov S, Fortov V E, Lipaev A M, Molotkov V I, Petrov O F, L wen H and Morfill G E 2010 *Phys. Rev. Lett.* **105** 045001
- [35] Vissers T, Wysocki A, Rex M, L wen H, Royall C P, Imhof A and van Blaaderen A 2011 *Soft Matter* **7** 2352–2356
- [36] McCandlish S R, Baskaran A and Hagan M F 2012 *Soft Matter* **8** 2527–2534
- [37] Cisneros L H, Cortez R, Dombrowski C, Goldstein R E and Kessler J O 2007 *Experiments in Fluids* **43** 737–753
- [38] Wolgemuth C W 2008 *Biophys. J.* **95** 1564–1574
- [39] Wensink H H, Dunkel J, Heidenreich S, Drescher K, Goldstein R E, L wen H and Yeomans J M 2012 Meso-scale turbulence in living fluids, submitted
- [40] Tirado M M, de la Torre J G and Martinez C L 1984 *J. Chem. Phys.* **81** 2047–2052
- [41] Cisneros L H, Kessler J O, Ganguly S and Goldstein R E 2011 *Phys. Rev. E* **83** 061907
- [42] Onsager L 1949 *Ann. N.Y. Acad. Sci.* **51** 627–659
- [43] Bialk  J, Speck T and L wen H 2012 *Phys. Rev. Lett.* to appear
- [44] Danilov S D and Gurarie D 2000 *Uspekhi Fizicheskikh Nauk* **170** 921–968
- [45] Kellay H and Goldburg W I 2002 *Rep. Prog. Phys.* **65** 845–894
- [46] Frisch U 2004 *Turbulence* (Cambridge: Cambridge University Press)
- [47] Kraichnan R H 1967 *Phys. Fluids* **10** 1417–1423
- [48] Kraichnan R H and Montgomery D 1980 *Rep. Prog. Phys.* **43** 547–619
- [49] Toner J and Tu Y 1998 *Phys. Rev. E* **58** 4828–4858
- [50] Toner J, Tu Y and Ramaswamy S 2005 *Ann. Phys.* **318** 170–244
- [51] Tailleur J and Cates M E 2008 *Phys. Rev. Lett.* **100** 218103
- [52] Rex M, Wensink H H and L wen H 2007 *Phys. Rev. E* **76** 021403
- [53] Wittkowski R and L wen H 2011 *Molecular Physics* **109** 2935–2943